Supporting Information for

Sustainable Off-grid Desalination of Hypersaline Waters by Janus Wood Evaporator

Xi Chen[1], Shuaiming He[2], Mark M. Falinski[1], Yuxi Wang[1,3], Tian Li[2], Sunxiang Zheng[1], Dongya Sun[1], Jiaqi Dai[2], Yanhong Bian[1], Xiaobo Zhu[1], Jinyue Jiang[1], Liangbing Hu[2]*, and Zhiyong Jason Ren[1]*

1 Department of Civil and Environmental Engineering and Andlinger Center for Energy and the Environment, Princeton University, Princeton, NJ 08544, United States.

2 Department of Materials Science and Engineering, University of Maryland, College Park, MD 20742, United States.

3 The Earth Institute and School of International and Public Affairs, Columbia University, New York, NY 10027, United States.

***Corresponding authors:**

Liangbing Hu: binghu@umd.edu;

Zhiyong Jason Ren: zjren@princeton.edu

This file includes:

Note 1.

Tree species and cutting directions

Basswood and Balsawood were tested in this study to choose the most suitable base material for the Janus wood evaporator. Two cutting directions, parallel or vertical to the growth direction, were studied to enhance solar desalination performance (Figure S3). All wood samples were placed on a hot plate at 500 °C for 45 s to carbonize the wood and generate the solar absorber surface (Figure S4). Parallel cutting of both Basswood and Balsawood showed aligned channel structures on the evaporative surface (Figure S5 a&c), where pits growing on vessel walls formed the vapor pathway for efficient solar steam generation. Meanwhile, the vertically cut samples of Basswood and Balsawood had abundant openings of different diameters (Figure S5 b&d), which linked the downward low-tortuosity channel structures. In the surface temperature test, parallelly-cut (P) samples outperformed vertically-cut (V) samples, indicating that P samples improved heat localization and increased solar-thermal conversion [1]. Meanwhile, Balsawood had a higher surface temperature than Basswood, credited to the higher porosity of Balsawood. However, the overall solar desalination performance of Basswood evaporators surpassed that of the Balsawood evaporator. This could be attributed to Basswood having enough pits for vapor transport, while Balsawood has fewer pits, which limited vapor permeate. From this preliminary test, we picked the parallelly-cut Basswood for the Janus wood evaporator.

Note 2.

Ion diffusivity in the wood structure

As has been reported, ion diffusion in a porous media filled with water could be hindered by the porous structure. As a result, it is worth investigating the effect of wood's intrinsic porous structure on the diffusion of NaCl in the hydrophilic part of the Janus wood evaporator.

The hindering effect could be very limited if the ratio between the solute radius and the channel size in the porous medium (r_s/R_p) is <0.01.[2] The radii of hydrated Na^+ in water is ~0.36 nm, the radii of hydrated Cl^- in water is ~0.33 nm,[3] and the smallest pore size in the wood structure is ~1 μm for the pits on vessel walls. Therefore:

for Na^+: $r_s/R_p \sim 3.6 \times 10^{-4}$

for Cl^-: $r_s/R_p \sim 3.3 \times 10^{-4}$

Both ratios were far less than 0.01, so the hindering of ion diffusion inside the pore structure in a wood evaporator could be reasonably neglected. Therefore, the apparent diffusivity (D_m) of NaCl in the wood structure was assumed to be very close to that in water. Or, in other words, the diffusion inside the hydrophilic part in the Janus wood evaporator could be as fast as that in the bulk brine.

Note 3.

Background of the LCA of Janus wood solar desalination system

While some existing literature presents relatively environmentally efficient zero liquid discharge systems,[4,5] those tend to study systems at a larger scale (e.g. 250 m^3 water/day vs 1 m^3 water/day) and/or consider a significantly lower influent feed concentration (e.g. < 0.2% vs. ~20%) than explored in this study. Further, some only consider the Scope 2 emissions in their study, without evaluating the Scope 3 emissions related to chemical and material inputs. Technologies used in these systems, such as reverse osmosis, tend to require exponentially higher energy requirements as influent concentration increases, as well as a decrease in water recovery,[6] which would lead to exponential increases in CO_{2e} per functional unit. Furthermore, these technologies, like many technologies, tend to see decreased impacts as they optimize the technology and scale up from the bench-scale or pilot-scale.[7,8]

Note 4.

Global inventory and assumptions

For all modeled Janus evaporator systems, there were global values that were selected such that each system was compared based on a similar benchmark. Table S2 shows the global assumptions that were consistent across each Janus evaporator system, while Table S3 shows material and energy inputs that were consistent across all systems. It is assumed that only one polyvinylchloride tank, one set of pipes, one inverter, and one pump is required over the course of a 20-year period, per system.

Tank volume for evaporator systems: It is assumed that all tanks for Janus evaporator systems are 2 cm tall, the walls are 0.25 cm thick, and that the tank is a square of the same dimensions as the Janus evaporator, so the length of each side would be the square root of the area of the Janus evaporator. It is also assumed that PVC has a density of 1340 kg/m^3. The volume of PVC required to build the tank is therefore represented by Equation S1:

$$PVC\ Volume\ (PVCv, m^3) = Evaporator\ Area * 0.0025 + 4 * (\sqrt{Evaporator\ Area} * 0.02 * 0.0025)$$

(Equation S1)

Pump power: The pumps used in Janus evaporator systems require so little energy (0.0072 kWh per day), that it is ultimately insignificant over the 20-year lifetime of the system. Therefore, a photovoltaic panel is included in each model to be more representative of the ideal situation for Janus evaporator use. The PV could easily be replaced by on-grid electricity, without any significant change to the results. To illustrate this, Figure S10 shows the GWP of a Janus wood evaporator system powered by on-grid electricity and electricity from a PV panel. There is no statistically significant difference in the resultant global warming potential.

Janus wood evaporator inventory and assumptions

Evaporation rate: To estimate evaporation rate (E.R.) of the Janus wood evaporator, the E.R. as a function of solar flux was assumed to be linear, and was estimated based on the data used to construct Figure 3h. Error in the slope and intercept of the linear regression equation was calculated based on the coefficient of determination.

Janus wood area, volume, and mass: The total area of the Janus wood needed over the course of a 20-year period is represented by Equation S1. Each variable is explained in Table S2 or Table S3, and the value of "1000" in the numerator represents the mass of treated water per day, in kg:

$$Janus\ wood\ area\ (JWA,\ m^2) = \frac{1000}{S * (Bef + Mef * P)} * \frac{7300}{Le} \quad \text{(Equation S2)}$$

The volume of Janus wood is given by Equation S2, where the thickness of wood is assumed to be 1 cm:

$$Janus\ wood\ volume\ (JWV, m^3) = 0.01 * Janus\ wood\ area \quad \text{(Equation S3)}$$

Also, Basswood has an average density of about 450 kg/m^3, so Equation S3 can be used to calculate the total mass of basswood required over the 20-year lifetime of the system:

$$Janus\ wood\ mass\ (JWM, kg) = 450 * Janus\ wood\ volume \quad \text{(Equation S4)}$$

Carbonization: Wood carbonization has been modeled in ecoinvent as a Process called "charcoal production | charcoal | Cutoff, U". Since carbonization and charcoal production are synonymous, the "charcoal production | charcoal | Cutoff, U" was modified for this study. The main modification was the removal of "hardwood" as an input Flow, since basswood is considered to be a "softwood", and is included elsewhere in the inventory. Further, since only roughly 10% of the Janus wood is carbonized, it was conservatively assumed that surface carbonization would require 50% of the energy and heat inputs of transforming the wood input into 100% charcoal.

Perfluorodecyltriethoxysilane (FAS): FAS is not an available Flow in ecoinvent v3.5, and its synthetic process is not reported. Instead, to determine the impacts from this molecule, proxy molecules were selected with similar chemical structures to represent each functional group emerging from the central Si (Figure S11). Dimethyldichlorosilane was chosen as a representative molecule for the central Si, mainly due to its use as a precursor to other silanes. Diethyl ether represented the ethyoxy groups and 2 perfluoropentane molecules represented the perfluorodecyl group, due to similarities in chemical structure. To be more conservative, it was assumed that 50% excess of each representative molecule was required to model one FAS molecule (i.e. 1.5 dimethyldichlorosilane molecules, 4.5 diethyl ether molecules, and 3 perfluoropentane molecules).

Wood heating: It was assumed that drying the wood after FAS application occurred in an industrial grade oven, specifically a 37.4 Cu. Ft. MEMMERT Forced Air Universal Oven, which has a maximum power of 7 kW, and a total volume of 1.05 m^3. This study assumed a drying time of 1 hour at maximum power, and that 75% of the oven volume is occupied

by Janus wood, yielding an energy requirement of 0.0198 kWh/kg wood, with a potential error of up to 20%.

Carbon nanotube:cellulose nanofiber aerogel evaporator inventory and assumptions

Evaporation rate: The reported E.R. was extracted from Figure 5d from Hu et al. and estimated at a value of 1.22 kg m^{-2} h^{-1} .[9] Note that this is the E.R. for an influent solution concentration of 12 wt%, which is lower than the influent concentration used in this study. This is also the E.R. at 1 kW/m^2 solar flux. Therefore, the actual E.R. used to estimate the required evaporator area is assumed to be the E.R. multiplied by the value for P.

Janus evaporator area, volume, and mass: The total area of the aerogel needed over the course of a 20-year period is represented by Equation S5. Each variable is explained in Table S2 or in the above section "Evaporation Rate", and the value of "1000" in the numerator represents the mass of treated water per day, in kg:

$$Aerogel\ evaporator\ area\ (AEA,\ m^2) = \frac{1000}{S * (1.22 * P)} * \frac{7300}{Le} \quad \text{(Equation S5)}$$

The volume of Janus wood is given by Equation S6, where the thickness of the aerogel is assumed to be 9 mm:

$$Aerogel\ evaporator\ volume\ (AEV, m^3) = 0.009 * Aerogel\ evaporator\ area \quad \text{(Equation S6)}$$

Also, the aerogel was estimated to have an average density of about 20 kg/m^3, so Equation S7 can be used to calculate the total mass of evaporator required over the 20-year lifetime of the system:

$$Aerogel\ evaporator\ mass\ (AEM, kg) = 20 * Aerogel\ evaporator\ volume \quad \text{(Equation S7)}$$

Nanomaterials: This aerogel evaporator was composed of three nanomaterials that do not exist in the ecoinvent v3.5 database: carbon nanotubes, cellulose nanofibers, and SiO_2 nanoparticles. Carbon nanotubes were modeled based on the synthesis process and life cycle inventory described in Healy et al.,[10] cellulose nanofibrils were modeled based on the synthesis process and life cycle inventory described in Arvidsson et al.,[11] and the SiO_2 nanoparticles were modeled based on the inventory featured in Roes et al.[12]

Aerogel freeze drying: The production of the CNT:CNF:SiO_2 evaporator required freeze drying, which can be a highly energy-intensive process. The energy requirements of industrial-grade freeze drying was modeled based on the Parker 10, 10 Cart Freeze Dryer, which has a shelf area of roughly 128.8 m^2, and operates at a power of 127 kW. This study assumed a "freeze dry time" (FDT) of 24-48 hours (with a mean of 36 hours) to freeze dry 128.8 m^2 of aerogel evaporator.

Electrospun Janus evaporator with carbon black

Evaporation rate: The reported E.R. was extracted from Figure S10 from Xu et al. and estimated at a value of 1.19 kg m^{-2} h^{-1}.[13] Note that this is the E.R. for an influent solution concentration of 20 wt%, which is the same as the influent concentration used in this study. This is also the measured E.R. at 1 kW/m^2 solar flux. Therefore, the actual E.R. used to estimate the required evaporator area is assumed to be the E.R. multiplied by the value for P.

Janus evaporator area, volume, and mass: The total area of the electrospun fibers needed over the course of a 20-year period is represented by Equation S8. Each variable is explained in Table S2 or in the above section "Evaporation Rate", and the value of "1000" in the numerator represents the mass of treated water per day, in kg:

$$Electrospun\ evaporator\ area\ (EEA,\ m^2) = \frac{1000}{S * (1.19 * P)} * \frac{7300}{Le} \qquad \text{(Equation S8)}$$

The volume of this Janus evaporator was not calculated since the thickness was never provided. Instead, it was reported that a total of 2.62E-4 kg PAN and 3.16E-3 kg PMMA were electrospun onto an area of 0.06 m^2, so the total mass of PAN and PMMA, in kg, is 4.37E-4 kg/m^2 and 0.0527 kg/m^2, respectively. Further, power requirements for electrospinning were estimated based on the Yflow FibeRoller Electrospinning Machine, with an estimated power draw of 1-2 kW (average: 1.5 kW, variable name: ELP). It was reported that is takes 3 h of electrospinning to produce a 0.06 m^2 mat in this study. Therefore, it would take 50 total hours to produce a 1 m^2 mat. Therefore, the energy required in electrospinning can be calculated by Equation S9:

$$Electrospun\ energy\ (ELE, kWh) = \text{ELP*50*EEA} \qquad \text{(Equation S9)}$$

Polymers and carbon black: PMMA was assumed to be well-represented by "polymethyl methacrylate sheets", and although the carbon black used in Xu et al. was at the nano-scale, it was assumed that those materials were well-represented by the "market for carbon black", and that the mass of carbon black was 5-10% (variable name: CB%) of the mass of electrospun polymer. Polyacrylonitrile (PAN) is not represented in ecoinvent and was therefore modeled based on the work of Das [14]. 1 kg PAN requires 0.952 kg acrylonitrile, 0.083 kg vinyl acetate, 4.15 kg dimethylacetamide, 0.220 mmBtu natural gas, and 0.77 kWh electricity.

Reverse osmosis system

Unlike the passive techniques described above, the use of a reverse osmosis system does not operate under the same global assumptions. The photovoltaic-powered reverse osmosis (PV-RO) system modeled here is based upon the work of Jijakli et al. who built

a simple LCA to evaluate the environmental impacts of PV-RO. As a result, much of the inventory from that study was used in this study. It is of note that there are a few assumptions from that study that do not translate well to this one, and as a result, those assumptions were modified and can be found below. Further, it has been noted that a very simple PV-RO system (which is modeled here) is likely not an ideal solution for the desalination of hypersaline water [15], and other solutions, such as pairing RO with other technologies [4], establishing multiple RO systems in tandem [16], or improving membrane materials, would be needed [17]. However, to match the simple, preliminary nature of the Janus evaporator inventories above, Jijakli et al.'s model was chosen [18], even if it is unlikely to be used in practice.

On-grid reverse osmosis (OG-RO) would have almost exactly the same inventory as the PV-RO system. The only difference would be that the electricity powering the pump would come from the on-grid power.

General model assumptions: It is assumed that the polypropylene, rubber and adhesives, anti-scalant, anti-foulant, lower energy pump, and PV inverter from the above evaporator models are consistent in this model. All other inventory can be found below in a modified form. Cellulose acetate does not appear in the ecoinvent database, and was instead modeled using ETH's FineChem tool.[19] Note that the mass of the cellulose acetate membrane and the mass of anti-scalant is assumed to remain constant, even though a larger mass of each would likely be required, as Jijakli et al.'s model assumes influent brackish water (<4%),[18] while the Janus wood model assumes an influent concentration of 20 wt% NaCl. However, the GWP impacts of each material are relatively insignificant relative to the final GWP of the entire system. Further, as the functional unit is related to ZLD, the RO system modeled here must have a 90-99% (average: 95%, variable name: Y) water recovery, with an effluent of drinking water quality (~100 ppm). The osmotic pressure was estimated by Equation S10 from the US Department of the Interior Bureau of Reclamation [20], where π_{NaCl} is the osmotic pressure of an influent solution of NaCl and M_{NaCl} is the molarity of the influent solution:

$$\pi_{NaCl}\,(kPa) = 351.15 * M_{NaCl}^{2} + 4365.18 * M_{NaCl} + 25.72 \qquad \text{(Equation S10)}$$

The energy required per m^3 water can be calculated with Equation S11, where SE is the specific energy at the thermodynamic restrictions (in kWh), M_{in} is the molarity of the influent solution, M_{eff} is the molarity of the effluent, π_{in} is the osmostic pressure (from Equation S10, in Pa), and η is the pump efficiency (assumed to be 75%):

$$SE = 2.7778 * 10^{-7} * \left(\frac{M_{in} - M_{eff}}{M_{in}}\right) * \frac{\pi_{in}}{\eta * Y * (1 - Y)} \qquad \text{(Equation S11)}$$

From this information, the PV panel size for the PV-RO can be estimated with Equation S12 under the assumption that its efficiency is 15%,[21] and it experiences the same hours of sunlight (S) and intensity of sunlight (P) as the Janus evaporators.

$$PVsize\,(m^2) = 0.007 + \frac{SE}{S * P * 0.15} \qquad \text{(Equation S12)}$$

Note 5.

The LCA of three RO-precipitation processes modeled by Roquim et al. for a much lower concentration (<0.2%) of a wider variety of salts were also used for comparing with the Janus wood system (Supplementary Figure S14). A Janus wood evaporator could outperform all three RO-precipitation systems when used more than 1800 times. In other words, the Janus wood has a chance to be more sustainable for ZLD than the RO-precipitation even in extremely low concentration circumstances, as long as the evaporator's lifetime is long enough.

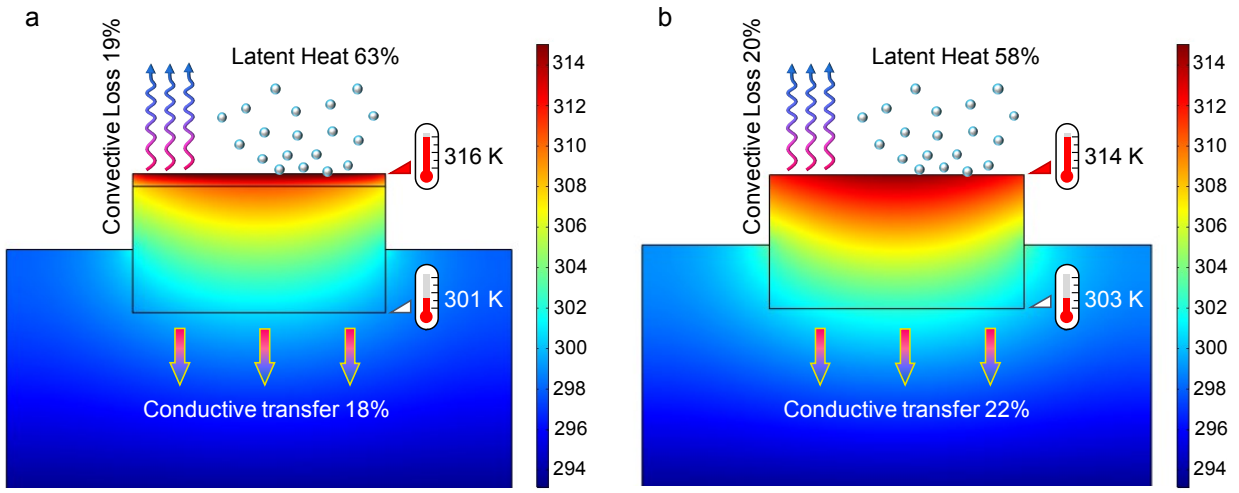

Figure S1. Temperature distribution in (a) the Janus wood evaporator with asymmetric wettability and (b) the natural wood evaporator with uniform wettability. Simulated using COMOSOL.

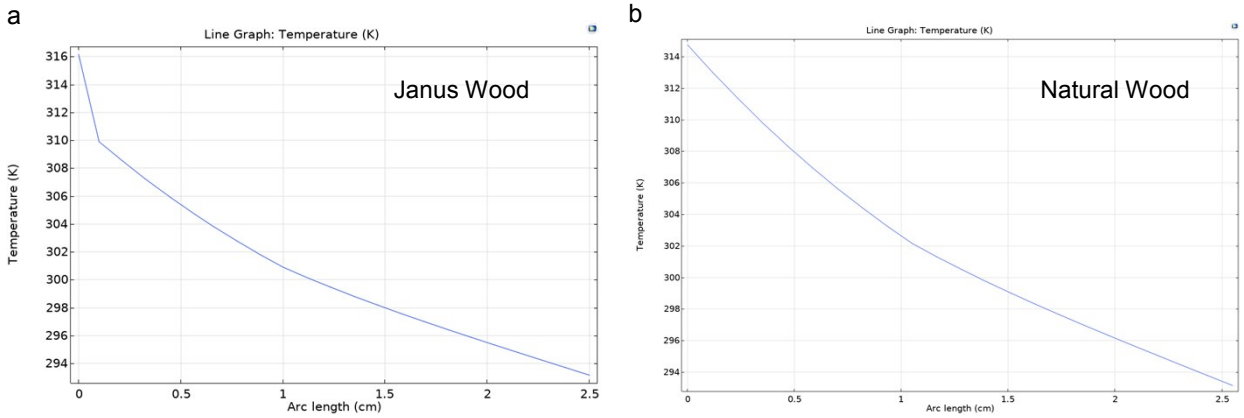

Figure S2. Temperature profile in (a) the Janus wood evaporator with asymmetric wettability and (b) the natural wood evaporator with uniform wettability. Simulated by COMSOL.

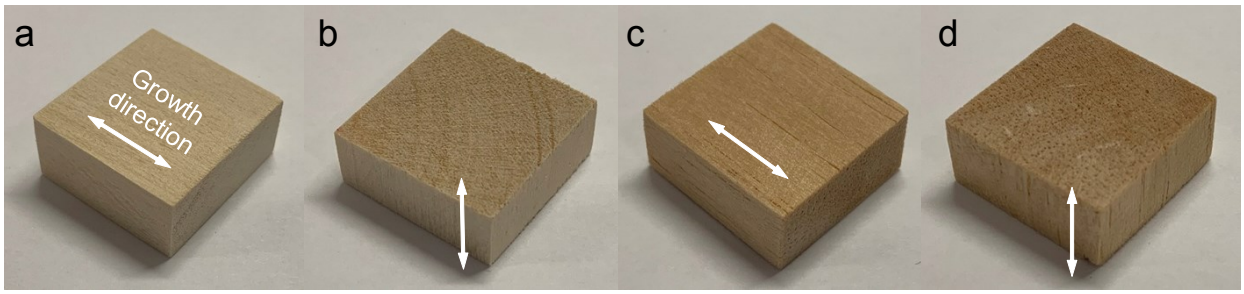

Figure S3. Different wood substrates prepared from Basswood and Balsawood cut in the parallel (P) and vertical (V) to growth direction. (a) Basswood in the parallel direction, (b) Basswood in the vertical direction, (c) Balsawood in the parallel direction, (d) Balsawood in the vertical direction.

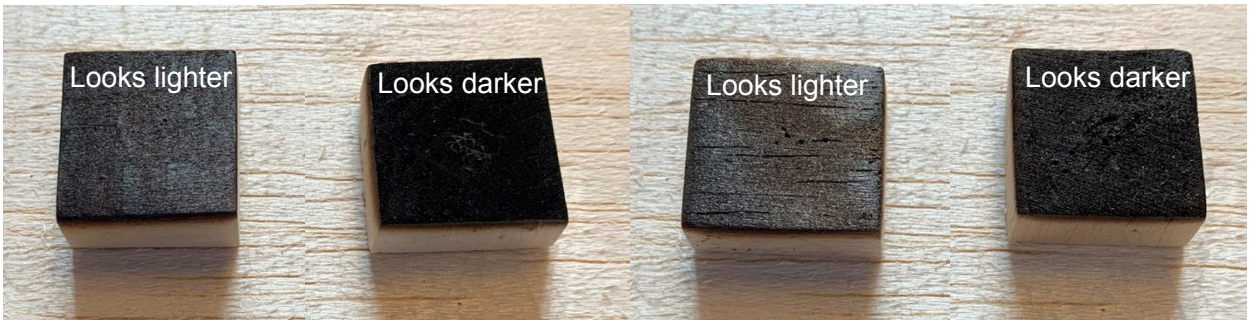

Figure S4. Optical investigation of the carbonized wood samples. P: cut parallelly to the growth direction; V: cut vertically to the growth direction.

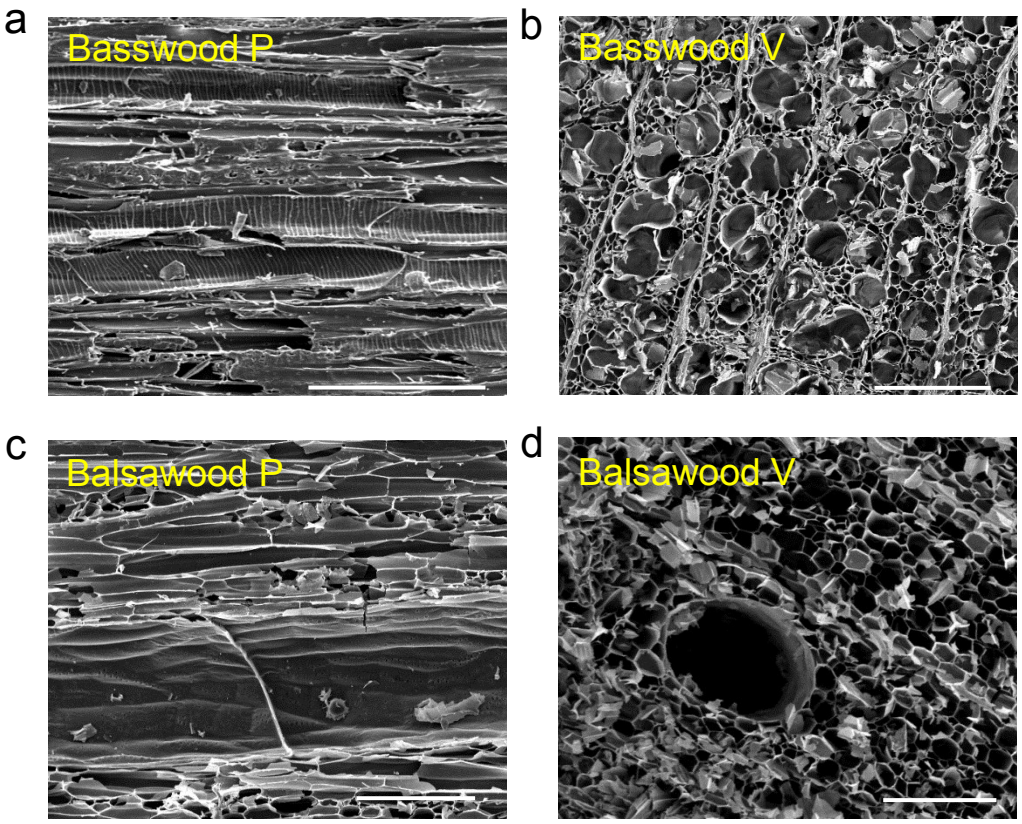

Figure S5. SEM images for (a) Basswood in the parallel direction, (b) Basswood in the vertical direction, (c) Balsawood in the parallel direction, and (d) Balsawood in the vertical direction.

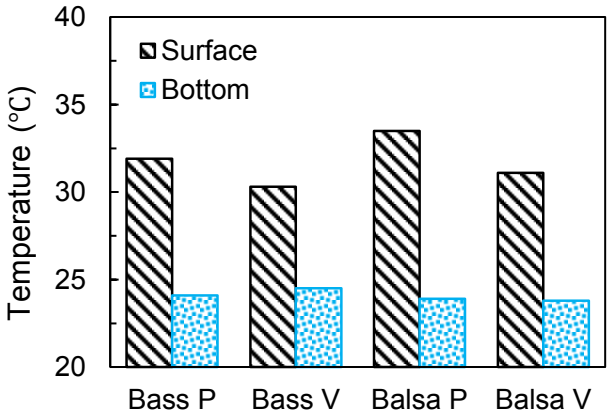

Figure S6. Surface temperature of different wood evaporator samples under 0.5 sun. P: cut parallelly to the growth direction; V: cut vertically to the growth direction.

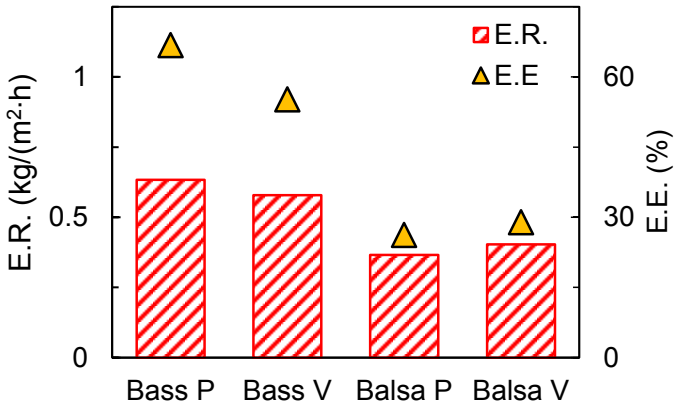

Figure S7. Evaporation rate (E.R.) and evaporation efficiency (E.E) of different wood evaporator samples under 0.5 sun.

Before FAS treatment After FAS treatment

Figure S8. Wettability of the wood evaporator before and after FAS treatment.

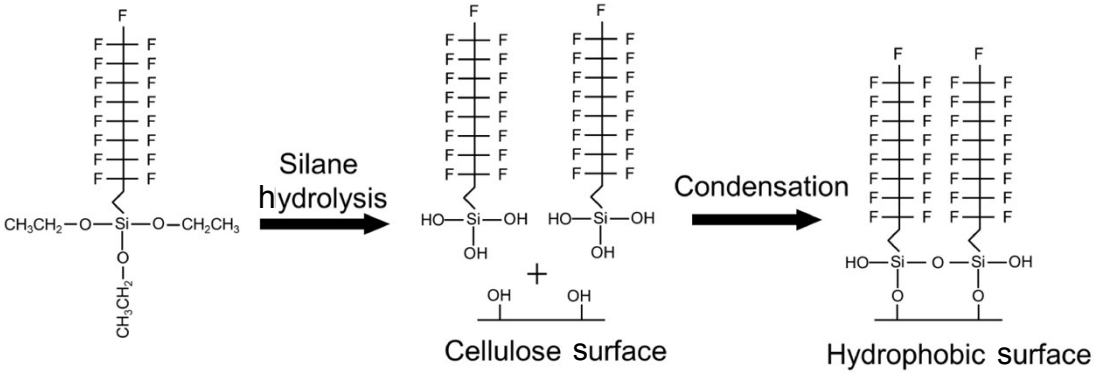

Figure S9. Mechanism of FAS treatment for the cellulose surface [22].

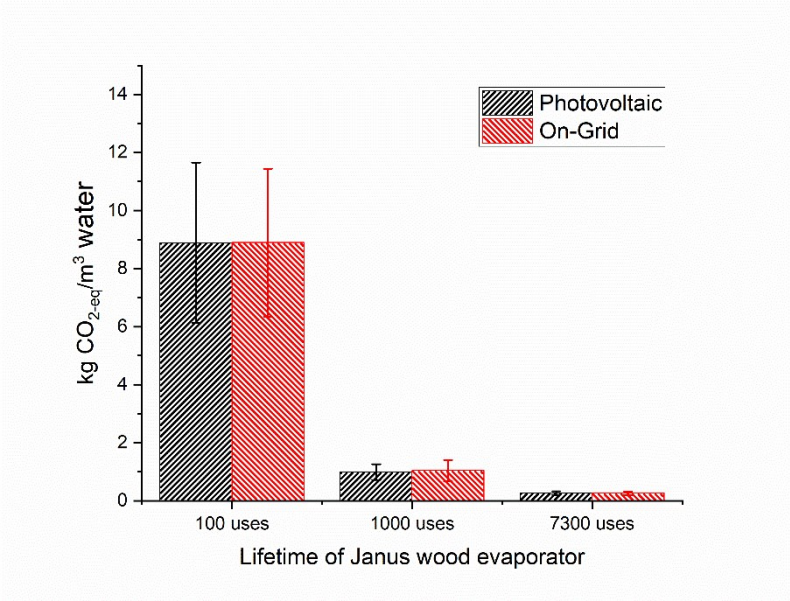

Figure S10. Global warming potential (in kg $CO_{2\text{-eq}}$/functional unit) of Janus wood evaporator systems powered by photovoltaic cells or by electricity found on the grid.

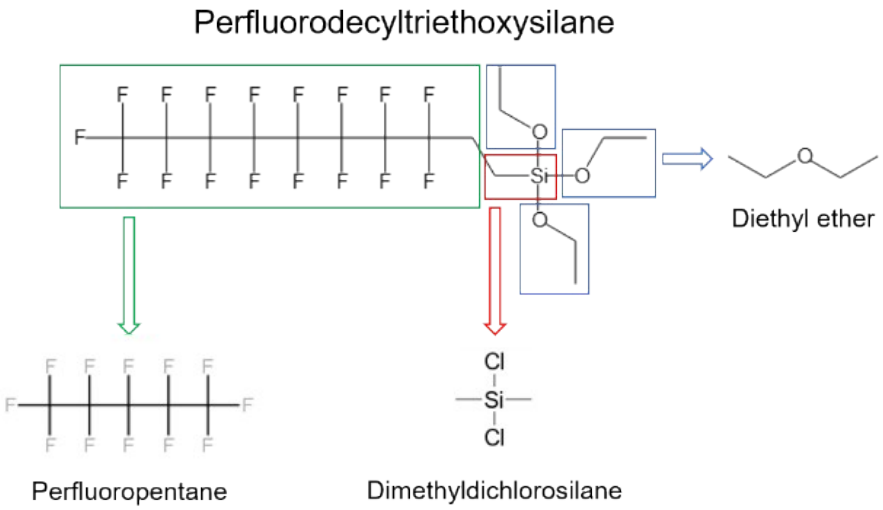

Figure S11. Image of perfluorodecyltriethoxysilane and the three molecules used in the LCA to approximate $CO_{2\text{-eq}}$ emissions.

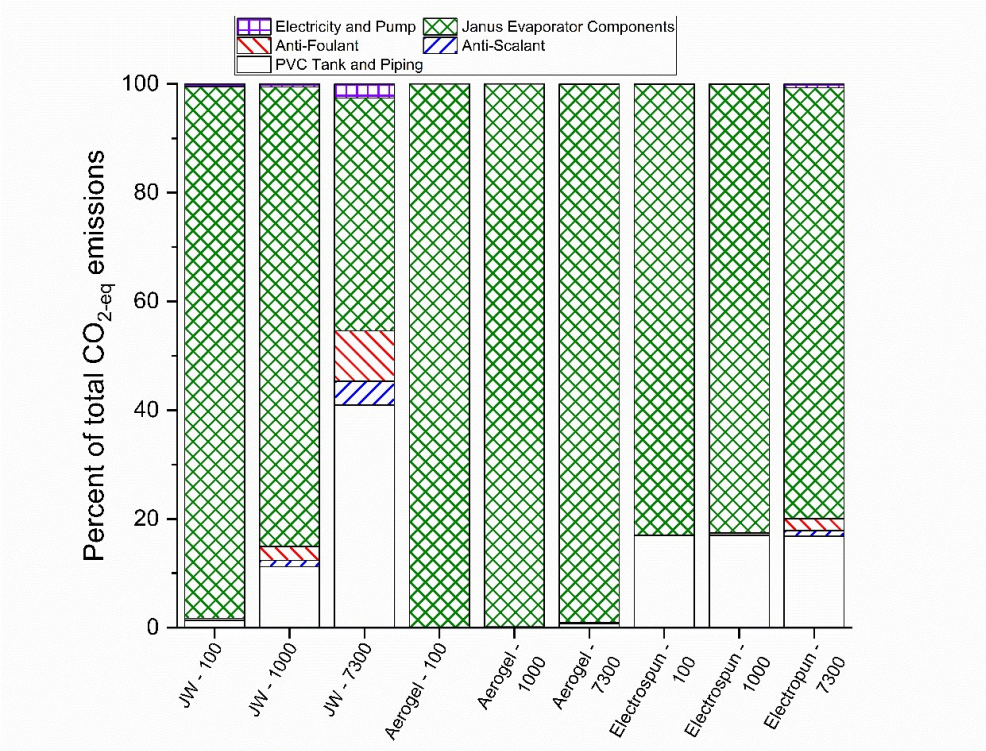

Figure S12. The percent of total $CO_{2\text{-}eq}$ emissions resulting from each part of the Janus Wood (JW), CNT:CNF aerogel, and electrospun evaporator systems for evaporator lifetimes of 100, 1000, or 7300 uses.

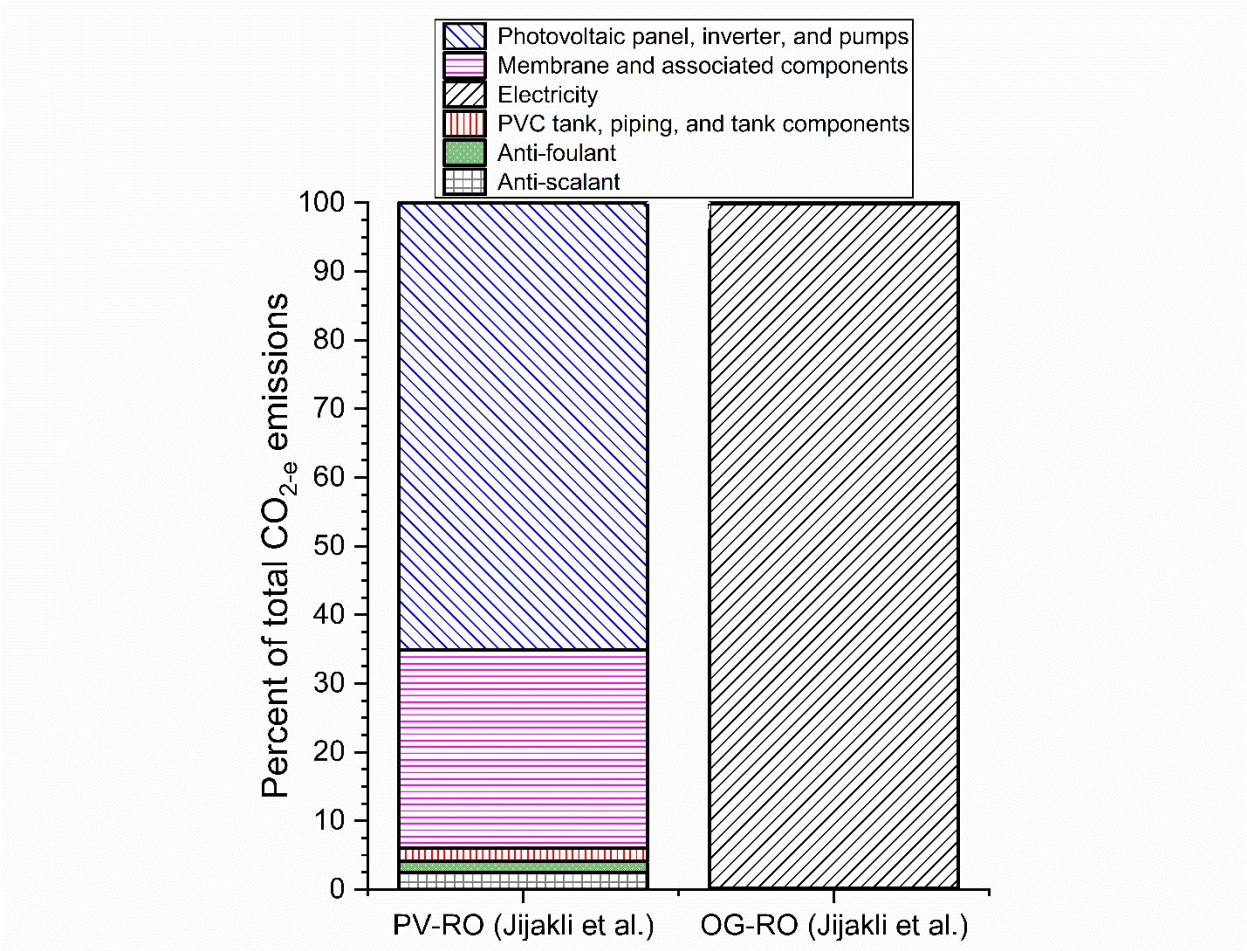

Figure S13. The percent of total CO_{2e} emissions resulting from each part of the photovoltaic-powered (PV-RO) and on-grid (OG-RO) powered reverse osmosis systems.

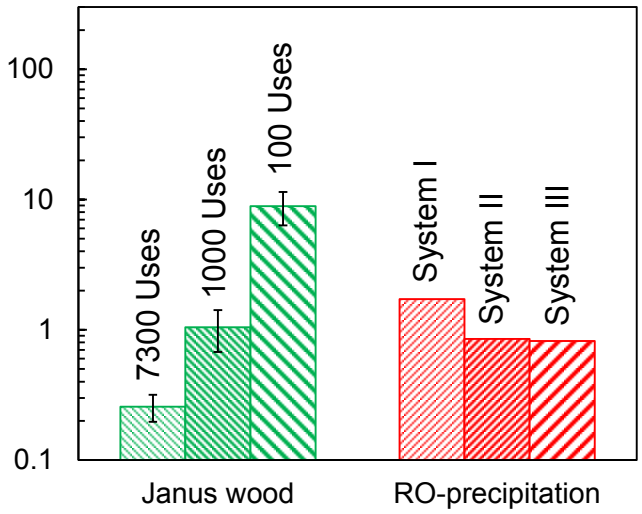

Figure S14. The global warming potential of the Janus wood evaporator and the RO-Precipitation systems.

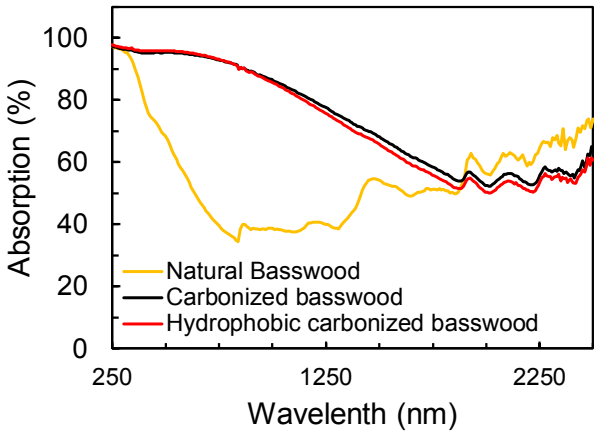

Figure S15. Solar absorption of the natural basswood, carbonized wood, and hydrophobic carbonized wood. The FAS treatment affected little on the optical property of the carbonized wood.

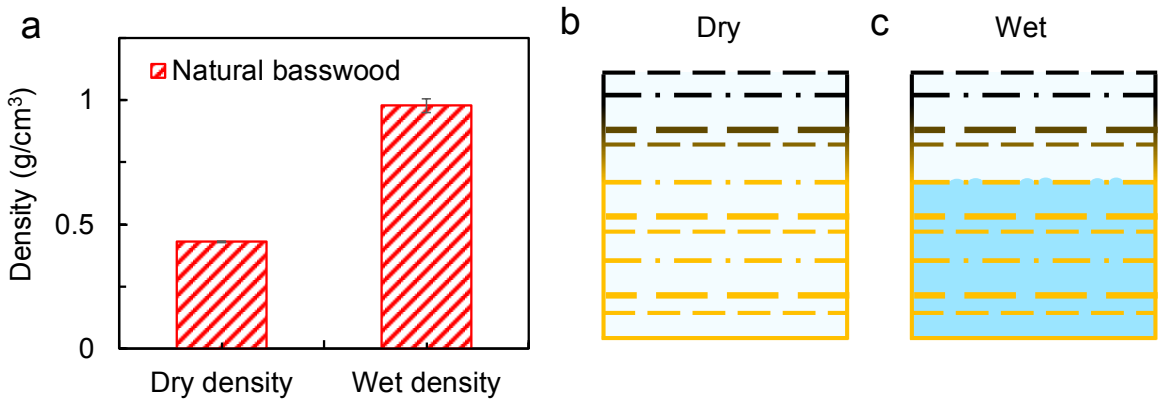

Figure S16. (a) Density of Basswood and Balsawood, and (b, c) the scheme of hydrophobic layer thickness measurement.

Table S1.

Comparison of reported solar evaporators with Janus wettability.

Materials			**Additional thermal insulation unit**	**Efficiency (1 sun)**	**Salinity**	**Ref.**
Substrate	**Solar absorber**	**Hydrophobization**				
Natural wood	**Carbonization**	**FAS treatment**	**No**	**92.3%** **87.6%** **84.3%** **82.0%**	**0%** **5%** **10%** **20%**	**Ours**
Polyacrylonitrile film	Carbon black nanoparticles	Polymethylmethacrylate	No	51%	3.5%	[13]
Single-walled CNT film	Au nanorods	Au nanorods	No	82%	0%	[23]
Cellulose ester filter membrane	Delaminated Ti_3C_2 nanosheet	FAS treatment	Yes	71%	2.75%	[24]
Cellulose nanofibers	Carbon nanotubes	Hexamethyldisilazane-treated SiO_2	No	83.3%	3.5%	[9]
Cotton fabric	Candle soot	Candle soot	No	53.7%	3.5%	[25]
Ultralong hydroxyapatite nanowires and glass fibers	Nickel oxide nanoparticles	Sodium oleate modification	Yes	83.5%	3.5%	[26]
Truss-like resorcinol-formaldehyde resin	Pyrolysis at 800 °C	Surface polymerization of dopamine and PFDTS treatment	No	74.2%	~3.5%	[27]

Table S2. Global assumptions and variables for Janus evaporators.

Functional unit:	Variable	Value	Error	Units
Influent volume	V	1	---	m^3/day
System lifetime	Ls	7300	---	days
Sunlight per day	S	8	1	hours
Solar flux at evaporator/PV panel	P	0.82	0.15	kW/m^2
Influent concentration (NaCl)	C	20	---	wt%
Evaporator lifetime	Le	100, 1000, 7300	---	days
Pump efficiency	η	75	---	%
PVC tank wall thickness	PVC_T	0.0025	---	m
PVC tank height	PVC_H	0.02	---	m
Photovoltaic efficiency	PV_e	15	---	%

Table S3. Constant inputs for each evaporator system, with an average functional unit of 1 m^3 hypersaline water treated per day over a 20-year period.

Constant inputs (per functional unit)	Functional use	Quantity	Units
Polyvinylchloride	Pipes	2.08E-3	kg
Silicon	Tank sealant	9.18E-5	kg
Polyethylene	Tank snsulation	4.66E-5	kg
Polycarboxylate	Anti-scalant	0.0187	kg
Sulfuric acid	Anti-foulant	0.112	kg
Inverter, 0.5 kW	PV panel inverter	1/7300	item
Pump, 40W	Water pump	1/7300	item

Table S4. Assumptions for average and uncertainty for Janus wood evaporator.

	Variable	Value	Error	Units
Evaporation rate slope	Mef	2.63	0.24	kg h^{-1} kW^{-1}
Evaporation rate intercept	Bef	-0.445	0.217	kg m^{-2} h^{-1}
Wood heating energy multiplier	X	100	20	%

Table S5. Inventory for a Janus wood evaporator.

Material/Energy input	Functional Use	Function or Value	Units
Electricity, medium voltage	Carbonization	0.075*156.1*JWM/2	kWh
Heat, central or small scale	Carbonization	0.720*156.1*JWM/2	MJ
Water, cooling	Carbonization	0.050*156.1*JWM/2	m3
Diethyl ether	FAS	0.0485*JWA	kg
Dimethyldichlorosilane	FAS	0.0282*JWA	kg
Electricity, medium voltage	Wood heating	X*0.0198*JWM	kWh
Ethanol	FAS application	4.22*JWA	kg
Perfluoropentane	FAS	0.1259*JWA	kg
Photovoltaic panel	Powering pump	0.007	m2
Polyvinylchloride	Water tank for Janus evaporator	PVCv*1340	kg
Sawnwood, board, softwood	Basswood	JWV	m3

Table S6. Inventory for an aerogel Janus evaporator.

Material/Energy input	Functional use	Function/Value	Units
Carbon nanotubes	Aerogel materials	AEM/2	kg
Cellulose nanofiber	Aerogel materials	AEM/2	kg
Electricity, low voltage	Freeze drying	127*FDT*AEA/128.8	kWh
Photovoltaic panel	Powering pump	0.007	m^2
Polyvinylchloride	Water tank for aerogel evaporator	PVCv*1340	kg
SiO_2 Nanoparticles	Aerogel materials	0.001*AEA	kg

Table S7. Inventory for an electrospun Janus evaporator.

Material/Energy input	Functional use	Function or value	Units
Acrylonitrile	PAN production	0.952*EEA*4.37E-4	kg
Carbon black	Carbonization	CB%*EEA* (4.37E-4+0.0527)	kg
Dimethylacetamide	Carbonization	4.15*EEA*4.37E-4	kg
Electricity, low voltage	PAN production	0.77*EEA*4.37E-4	kWh
Electricity, low voltage	Electrospinning	ELE	kWh
Electricity, low voltage	Vacuum oven	5.07*EEA	kWh
Heat, district or industrial	PAN production	2.2E-4*EEA*4.37E-4	kg
N,N-dimethylformamide	Electrospinning solvent	EEA*(12.5*4.37E-4+ 10*0.0527)	kg
Photovoltaic panel	Powering pump	0.007	m^2
Polyvinylchloride	Water tank for electrospun evaporator	PVCv*1340	kg
Vinyl acetate	PAN production	0.083*EEA*4.37E-4	kg

Table S8. Inventory for a reverse osmosis system, with energy source from photovoltaic panels or on-grid electricity.

Material/Energy input	Functional use	Function or value	Units
**Electricity, low voltage	Power for pumps	0.0072 + SE/7300	kWh
Glass fiber reinforced plastic, polyamide	RO module casing	1.93E-3	kg
Glass fiber reinforced plastic, polyester	RO module housing unit	5.92E-2	kg
*Inverter, 0.5 kW	PV panel inverter	1/7300	items
*Photovoltaic panel, CIS	PV panel for power	PVsize/7300	m^2
Polycarboxylates	Anti-scalant	0.0187	kg
Polyvinyl chloride	Low-pressure pipes	1.39E-3	kg
Pump, 40 W	Low-pressure water pump	1/7300	items
Seal, natural rubber based	O-rings	6.85E-5	kg
Steel, low alloyed	High-pressure pipes	3.72E-3	kg
Sulfuric acid	Anti-foulant	0.112	kg
Textile, knit cotton	Permeate spacer	5.75E-4	kg
Textile, non-woven polypropylene	Feed spacer	6.30E-4	kg
Water pump, 22 kW	High-pressure water pump	1/7300	items

* only present in the PV-RO system, ** only present in the OG-RO system

References

1 T. Li, H. Liu, X. Zhao, G. Chen, J. Dai, G. Pastel, C. Jia, C. Chen, E. Hitz, D. Siddhartha, R. Yang and L. Hu, *Adv. Funct. Mater.*, 2018, **28**, 1–8.

2 R. E. Beck and J. S. Schultz, *Science (80-.).*, , DOI:10.1126/science.170.3964.1302.

3 J. N. Israelachvili, *Intermolecular and Surface Forces: Third Edition*, 2011.

4 F. M. Ronquim, H. M. Sakamoto, J. C. Mierzwa, L. Kulay and M. M. Seckler, *J. Clean. Prod.*, , DOI:10.1016/j.jclepro.2019.119547.

5 S. P. Rajakumari and S. Kanmani, *J. Sci. Ind. Res. (India).*

6 T. V. Bartholomew, L. Mey, J. T. Arena, N. S. Siefert and M. S. Mauter, *Desalination*, , DOI:10.1016/j.desal.2017.04.012.

7 F. Piccinno, R. Hischier, S. Seeger and C. Som, *J. Clean. Prod.*, , DOI:10.1016/j.jclepro.2016.06.164.

8 C. Tristán, M. Rumayor, A. Dominguez-Ramos, M. Fallanza, R. Ibáñez and I. Ortiz, *Sustain. Energy Fuels*, , DOI:10.1039/d0se00372g.

9 R. Hu, J. Zhang, Y. Kuang, K. Wang, X. Cai, Z. Fang, W. Huang, G. Chen and Z. Wang, *J. Mater. Chem. A*, , DOI:10.1039/c9ta01576k.

10 M. L. Healy, L. J. Dahlben and J. A. Isaacs, *J. Ind. Ecol.*, , DOI:10.1111/j.1530-9290.2008.00058.x.

11 R. Arvidsson, D. Nguyen and M. Svanström, *Environ. Sci. Technol.*, , DOI:10.1021/acs.est.5b00888.

12 A. L. Roes, L. B. Tabak, L. Shen, E. Nieuwlaar and M. K. Patel, *J. Nanoparticle Res.*, , DOI:10.1007/s11051-009-9819-3.

13 W. Xu, X. Hu, S. Zhuang, Y. Wang, X. Li, L. Zhou, S. Zhu and J. Zhu, *Adv. Energy Mater.*, , DOI:10.1002/aenm.201702884.

14 S. Das, *Int. J. Life Cycle Assess.*, , DOI:10.1007/s11367-011-0264-z.

15 D. M. Davenport, A. Deshmukh, J. R. Werber and M. Elimelech, *Environ. Sci. Technol. Lett.*, , DOI:10.1021/acs.estlett.8b00274.

16 R. Y. Ning and T. L. Troyer, *Desalination*, , DOI:10.1016/j.desal.2007.11.060.

17 Z. Wang, A. Deshmukh, Y. Du and M. Elimelech, *Water Res.*, , DOI:10.1016/j.watres.2019.115317.

18 K. Jijakli, H. Arafat, S. Kennedy, P. Mande and V. V. Theeyattuparampil,

Desalination, , DOI:10.1016/j.desal.2011.09.038.

19 G. Wernet, S. Hellweg and K. Hungerbühler, *Int. J. Life Cycle Assess.*, , DOI:10.1007/s11367-012-0404-0.

20 US Department of the Interior Bureau of Reclamation and Sandia National Laboratories, *DESALINATION AND WATER PURIFICATION TECHNOLOGY ROADMAP*, 2003.

21 M. A. Green, *Nat. Energy*, 2016.

22 D. Hou, T. Li, X. Chen, S. He, J. Dai, S. A. Mofid, D. Hou, A. Iddya, D. Jassby, R. Yang, L. Hu and Z. J. Ren, *Sci. Adv.*, , DOI:10.1126/sciadv.aaw3203.

23 Y. Yang, X. Yang, L. Fu, M. Zou, A. Cao, Y. P. Du, Q. Yuan and C. H. Yan, *ACS Energy Lett.*, , DOI:10.1021/acsenergylett.8b00433.

24 J. Zhao, Y. Yang, C. Yang, Y. Tian, Y. Han, J. Liu, X. Yin and W. Que, *J. Mater. Chem. A*, , DOI:10.1039/c8ta05569f.

25 S. Gao, X. Dong, J. Huang, J. Dong, F. Di Maggio, S. Wang, F. Guo, T. Zhu, Z. Chen and Y. Lai, *Glob. Challenges*, , DOI:10.1002/gch2.201800117.

26 D. D. Qin, Y. J. Zhu, R. L. Yang and Z. C. Xiong, *Nanoscale*, , DOI:10.1039/c9nr10357k.

27 H.-Y. Zhao, J. Zhou, Z.-L. Yu, L.-F. Chen, H.-J. Zhan, H.-W. Zhu, J. Huang, L.-A. Shi and S.-H. Yu, *Cell Reports Phys. Sci.*, , DOI:10.1016/j.xcrp.2020.100074.